Aerosol and Air Quality Research, 18: 2879–2894, 2018

ISSN: 1680-8584 print / 2071-1409 online
doi: 10.4209/aaqr.2018.06.0239

Urban-scale SALSCS, Part II: A Parametric Study of System Performance

Qingfeng Cao[1], Minghua Huang[2], Thomas H. Kuehn[1], Lian Shen[1], Wen-Quan Tao[2], Junji Cao[3], David Y.H. Pui[1,2,4*]

[1] *Department of Mechanical Engineering, University of Minnesota, Minneapolis, Minnesota 55455, USA*
[2] *Xi'an Jiaotong University, Xi'an, Shaanxi 710049, China*
[3] *Key Lab of Aerosol Chemistry & Physics, Institute of Earth Environment, Chinese Academy of Sciences, Xi'an, Shaanxi 710061, China*
[4] *School of Science and Engineering, Chinese University of Hong Kong, Shenzhen, Guangdong 518172, China*

ABSTRACT

Following the experimental and numerical investigations of the Xi'an demonstration unit in Part I, Part II presents a parametric study on the proposed urban-scale SALSCS by using the validated numerical model. This study is aimed at understanding the influence of different variables on system performance, namely, the solar irradiation, ambient-air temperature and ground temperature at a 2-m depth as ambient parameters, and the inlet and outlet heights of the solar collector, collector width, tower width and tower height as geometric parameters. The effect of pressure drop across the filters on the system flow rate has been evaluated as well. The parameters that considerably influence the system performance have been identified.

Keywords: SALSCS; Air pollution remediation; Ambient parameters; System dimensions; Solar chimney.

INTRODUCTION

With its rapid growth in economy and industry, air pollution in China has become a commonly recognized issue as reported by many researchers (He *et al.*, 2003; Watts, 2005; Chan and Yao, 2008; Kan *et al.*, 2012; Huang *et al.*, 2014; Zhao *et al.*, 2016). On January 13, 2013, Beijing suffered an air pollution episode with average $PM_{2.5}$ concentration of 755 μg m^{-3}, more than 20 times higher than the daily $PM_{2.5}$ standard of 35 μg m^{-3} as promulgated by the U.S. Environmental Protection Agency (USEPA) (Federal Register, 2006). Song *et al.* (2017) studied air quality monitoring data among 31 provinces of the country from January 2014 to December 2016, and concluded that annual population-weighted average $PM_{2.5}$ concentration in China is 65.8, 55.0 and 50.7 μg m^{-3} during 2014, 2015 and 2016, respectively, indicating the improvement of the country's air quality during the last three years. However, they also found that $PM_{2.5}$ pollution during the winter seasons in the northern China became worse. Zhang *et al.* (2017) suggested, since 2007, there was a 10–20% decrease in China's exported particulate matter (PM) pollution towards its east coast except for winter seasons, but air pollution would still be an issue of the country for a long time. Numerous scientific studies have revealed that exposure to $PM_{2.5}$ has detrimental impacts on human health, such as cardiovascular and respiratory diseases, harming nervous system, and impeding neuropsychological development of children (Brook *et al.*, 2010; Genc *et al.*, 2012; Becerra *et al.*, 2013; Hoek *et al.*, 2013; Suades-González *et al.*, 2015; Guan *et al.*, 2016).

China has taken measures to prevent air pollution from impacting public health. Control strategies of air pollution include limiting emissions of SO_2, nitrogen oxides and particulate matter, tightening regulations for air pollution, proposing policies on energy conservation and emission reduction, strengthening supervision of law enforcement, developing cleaner and renewable energy resources (Feng and Liao, 2016; Gao *et al.*, 2016). As mentioned by Sun *et al.* (2016), tight limitations on personal car use were imposed in Beijing and its neighboring cities, and nearby factories and construction sites were ordered to close to reduce air pollution concentrations of the city during the Asia-Pacific Economic Cooperation (APEC) meeting in 2014, which were considered to be a costly and short-term approach. Yu (2014) proposed an interesting and bold approach of spraying water into the atmosphere from top of high buildings and scavenging air pollution in cities. A Solar-Assisted Large-Scale Cleaning System (SALSCS) was introduced by Cao *et al.* (2015) as a unique approach

* Corresponding author.
Tel.: +1 6126252537; Fax: +1 6126256069
E-mail address: dyhpui@umn.edu

to remediate urban air pollution. Its working principle has been introduced in Part I of this paper, which is similar to the Solar Chimney (SC) system. Since the proposal of SALSCS, attentions have been attracted in the academia field, with similar air pollution control strategies published in a few papers recently. Zhou *et al.* (2015) introduced a method of utilizing the SC configuration to generate updraft airflow with heating effect of urban heat island, and transport the ambient polluted air directly into higher atmospheric levels above the planetary boundary layer through a high system tower. However, no filters are contained in their proposed system. Tan *et al.* (2017) presented an idea of a filter-contained urban updraft tower (FUUT), which is driven by urban heat island effect instead of solar energy. Filters are installed to remove particulate matter in the atmosphere. Gong *et al.* (2017) further modified the SC tower geometry to be an inverted *U*-shape cooling tower and a water-spray system was proposed to be installed to strengthen the driving force of airflow. Filters were applied to clean particulate matter in their system as well. There are also ideas of combining SCs with large-scale photocatalytic reactors for removal of CO_2 and N_2O, respectively, to resolve the global warming issue (de Richter *et al.*, 2013; Ming *et al.*, 2016). Therefore, the authors of this paper believe that the method of applying SALSCS or similar systems to remediate urban air pollution is promising and will lead many new investigations to be conducted in the near future.

The urban-scale SALSCS introduced in this paper is aimed to improve the air pollution cleaning efficiency of the full-scale SALSCS proposed by Cao *et al.* (2015). According to the numerical study of Cao *et al.* (2018), eight full-scale systems installed in the suburb area of the Beijing city could mitigate air pollution by 11–15% over its urban regions. Compared to the full-scale SALSCS, the urban-scale unit has much smaller geometric dimensions of between 10 m and 120 m for both the tower height and solar collector width, so that many of them can be directly built inside a city to remove air pollutants and deliver clean air for urban residents.

Given SALSCS utilizes the SC configuration to generate updraft airflow with solar energy, geometric dimensions of the system and ambient parameters have important influence on its performance, which has been indicated by many investigations carried out on various SC systems. A two-dimensional numerical model was developed by Maia *et al.* (2009) to simulate the airflow field inside an SC under an unsteady condition, and results showed that the tower height and diameter were the two parameters affecting the system flow field most significantly. Zhou *et al.* (2009) derived a theoretical model to analyze effects of chimney height on the power output performance of Solar Chimney Power Plant (SCPP), and concluded that there existed an optimal chimney height which provides maximum power output. Kasaeian *et al.* (2011) conducted experimental measurements on a pilot SCPP. Flow and temperature fields inside the SCPP were analyzed and compared during both warm and cold days to understand effects of ambient temperature on system performance. However, they did not take variations of solar irradiation values during the two days into consideration. Two-dimensional numerical simulations were performed by Ming *et al.* (2011) to study effects of chimney configuration on the SCPP system characteristics parameters. It was found that cylindrical chimney contributed to better system performance than the divergent and conical chimneys. The height-to-diameter ratio of a chimney was studied as well, and its optimum value should range from 6 to 8. Li *et al.* (2012) proposed a theoretical model to analyze how SCPP power output changes with collector radius and chimney height. The analysis indicated that system power output increased with both the two variables, but there was a limitation on the power output when collector radius was increased over a certain range. Three-dimensional numerical simulations were carried out by Ming *et al.* (2012) to study the influence of ambient crosswind on SCPP. The major finding was that weak ambient crosswind had negative impact on the flow field and output power while strong wind could even increase the system's output power. Patel *et al.* (2014) investigated influences of various geometric parameters on an SCPP with fixed chimney height and collector diameter of 10 m and 8 m, respectively, by using three-dimensional numerical model. The studied geometric parameters included collector inlet and outlet heights, collector outlet diameter, chimney divergence angle and chimney throat diameter. A small SC pilot models were presented by Ghalamchi *et al.* (2015), with solar collectors of 3 m in diameter and chimney of 2 m in height. Measurements on the system temperature and velocity were carried out under different weather conditions. Maximum air velocity was recorded to be 1.3 m s^{-1} in the chimney and maximum temperature difference between the ambient and system airflow was measured to be 26.3°C. Later, Ghalamchi *et al.* (2016) set up a pilot SC system with a 3-m diameter solar collector and a 3-m height chimney. By experimentally changing the geometric dimensions, they found that 6 cm was the best dimension for collector inlet height of the setup, the chimney diameter had strong influence on the system performance, and the optimum value of around 3 m of the chimney height gave the best system performance. Three-dimensional numerical simulations were conducted by Kasaeian *et al.* (2017) with turbine blades resolved in the computational domain. Effects of parameters including turbine rotational speed, number of turbine blades, collector diameter and chimney height were investigated. Hassan *et al.* (2018) conducted numerical studies on the effects of solar collector slope and chimney diverging angel on the performance of Manzanares SC. It was found that by increasing collector slope appropriately, system flow rate can be enhanced, but a much larger slope may reduce the system overall performance as well. Meanwhile, the study indicated system power output can also be improved significantly by applying a chimney diverging angle at 1°. Ayadi *et al.* (2018) built up an SC with chimney height of 30 m and solar collector diameter of 27.5 m in Tunisia. Airflow temperature and velocity inside the system were recorded experimentally, and a numerical model was developed to investigate influence of collector roof height

on its performance characteristics. The authors stated that a lower collector roof height produces higher system power output. However, no systematic parametric investigation for the urban-scale SALSCS within the dimensional scale between 10 m and 120 m has been done so far in the research community.

This Part II paper presents a parametric study on how different ambient and geometric variables affect the system performance, which provides thoughtful guidance for system design and construction of urban-scale SALSCSs in the future. The simulations described here were conducted by using the numerical method presented in Part I, which has been validated against the measurement data on the demonstration unit in Xi'an. The studied ambient parameters include solar irradiation, ambient air temperature and 2-m deep ground temperature, while dimensional variables related to the SALSCS geometry are solar collector inlet and outlet heights, solar collector width, tower width and tower height. Effect of ambient wind on the system performance is not in the scope of the current study, since the model domain should then include the atmosphere near SALSCS. The latter requires a different numerical model and other experimental measurements with different set-ups for model validation. The rest of this paper is organized as follows. In Section 2, computational domain and boundary conditions of the numerical model for the urban-scale SALSCS are introduced. The influence of ambient and geometric variables on system performance is then presented and discussed based on the obtained numerical results. Detailed analysis is conducted to identify the most influential parameters on the system airflow rate and temperature field. At the end, a summary of the current investigation is given and future work related to the urban-scale SALSCS is suggested by the authors.

NUMERICAL MODEL OF URBAN-SCALE SALSCS

The governing equations, applied numerical schemes and meshing strategy of the urban-scale SALSCS model are consistent with the numerical model of the Xi'an demonstration unit as presented in Part I, which has been validated against experimental data obtained from the measurements during January 2017. The Xi'an demonstration unit has a tower of 60 m in height and a solar collector of 43×60 m^2 in horizontal dimensions. Therefore, it is right within the dimensional scale range of 10–120 m of the urban-scale SALSCS. Fig. 1 shows an example of the geometry of an urban-scale SALSCS, which is composed of a square solar collector and a rectangular prism tower, making it more simplified than the geometry of the Xi'an demonstration unit. Because of the symmetry of the geometry, the computational domain of an urban-scale SALSCS model was reduced to only a quarter of the system, with symmetric boundary conditions applied on the two sides of the domain as shown in Fig. 2. Similar with the Xi'an demonstration unit, the fan boundary condition is located at the mid-way between the solar collector inlet and center of the tower, and filters were simulated as an interface with a constant pressure drop. All boundary conditions are labeled by numbers in Fig. 2. Details of each boundary type can be referred to Table 1 in Part I, except for Boundary 5 which represents symmetry planes instead of partition walls. This model was applied to perform the parametric study on urban-scale SALSCS, in which ambient pressure was set to 101,325 Pa for all simulations, and ambient temperature, solar irradiation and 2-m deep ground temperature were varied case by case to evaluate their effects on the system performance. Air properties applied in each simulation were chosen according to the specific ambient temperature.

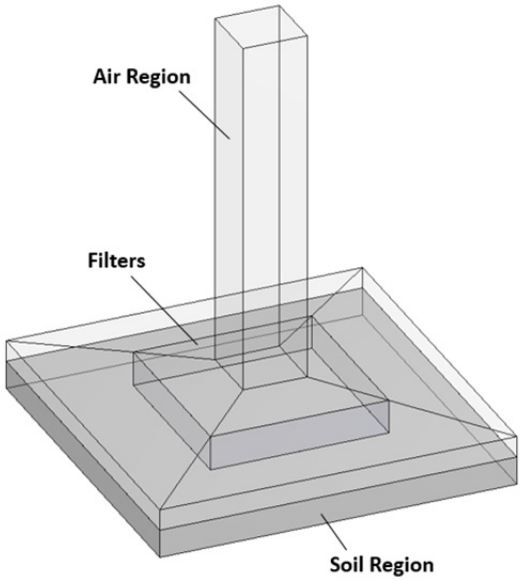

Fig. 1. Geometry of an urban-scale SALSCS with a 2-m thick soil layer underneath.

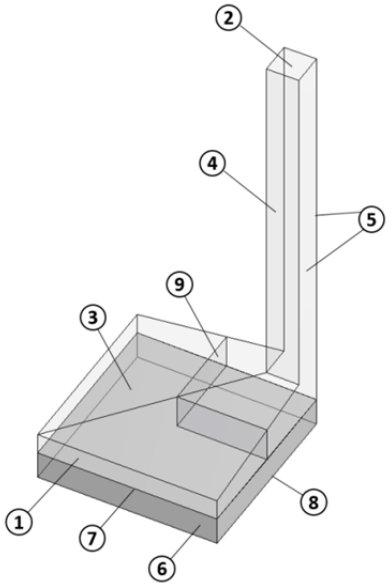

Fig. 2. Computational domain of the numerical model for urban-scale SALSCS. Boundary conditions labeled by the numbers correspond to Table 1 in Part I, except for Boundary 5.

RESULTS AND DISCUSSION

Effects of Ambient Parameters

Solar Irradiation

Numerical simulations were conducted on three urban-scale SALSCSs with different geometric dimensions. For each system, the tower height and collector width have the same dimensional value of 25 m, 50 m, or 75 m. The other geometric dimensions are same for all the three simulated SALSCSs, which are described in this section. The collector height increases from 1.5 m at the inlet to 3 m at the outlet (or tower base), while the width of the system tower is fixed at 5 m. To study the influence of solar irradiation on system performance, the ambient and 2-m deep ground temperatures were set to be 0°C and 4°C, respectively. We tested ambient solar irradiation values from 20 W m^{-2} to 1000 W m^{-2}. Fig. 3(a) shows that the system flow rate increases with the ambient solar irradiation significantly for all the three urban-scale SALSCSs. By changing the solar irradiation value from 20 W m^{-2} to 1000 W m^{-2}, the system flow rate is increased by 45.0 m^3 s^{-1}, 90.0 m^3 s^{-1} and 133.0 m^3 s^{-1} for the three systems with same tower and collector dimensions of 25 m, 50 m and 75 m, respectively. A system with smaller dimensional scale has both the flow rate value and flow rate increasing gradient lower than a larger system, indicating that the system geometric dimension is another factor affecting the SALSCS flow rate. For each curve in Fig. 3(a), flow rate at a lower ambient solar irradiation has a higher increasing gradient, due to that at a higher solar irradiation, the system is actually heating a larger amount of airflow, causing a lower enhancement rate with solar heating for the system flow rate.

The average airflow temperature at the tower outlet is an indication of the temperature field inside the urban-scale SALSCS. Profiles of this temperature are plotted in Fig. 3(b) as a function of solar irradiation for the three system dimensions. An increase in solar irradiation leads to a rapid increase in SALSCS airflow temperature for each system. With a solar irradiation increasing from 20 W m^{-2} to 1000 W m^{-2}, the airflow temperature at the tower outlet is 0.5–6.9°C, 1.0–14.0°C and 1.4–20.7°C higher than the ambient temperature of 0°C for the three system dimensions, respectively. Since a SALSCS with a larger solar collector area receives more solar energy, the corresponding airflow temperature is higher than for a system with a smaller collector area, which is also illustrated in Fig. 3(b).

Figs. 4(a) and 4(b) present the velocity contours and vector plots of the simulated airflow fields inside a system with the same tower height and collector width of 25 m under two solar irradiation values of 200 W m^{-2} and 600 W m^{-2}, respectively. As indicated by the contour figures, the region at the lower section of the system tower has the highest airflow velocity in the entire flow domain. For the system dimension of 25 m in both tower height and solar collector length, the maximum velocity values equal to 2.1 m s^{-1} and 3.0 m s^{-1} under the two solar irradiation values of 200 W m^{-2} and 600 W m^{-2}, respectively. Contour plots of the temperature and gauge static pressure fields under the two solar irradiation values are shown in Figs. 5(a) and 5(b), respectively, where gauge static pressure is defined as the difference between the airflow static pressure and the atmospheric pressure of 101,325 Pa. Comparison between the two figures indicates that the airflow field receiving more solar energy has a higher overall temperature, which agrees with the conclusion made from Fig. 3(b). Since the air flows at a higher velocity under a higher dynamic pressure for the solar irradiation of 600 W m^{-2} than for 200 W m^{-2}, lower flow static pressure field is achieved for the computational domain for the higher solar irradiation value.

Ambient Temperature

Ambient temperature values from –20°C to 30°C were tested in the current study, while solar irradiation was fixed at 300 W m^{-2} and the 2-m deep ground temperature was set to be 4°C higher than the corresponding ambient temperature for all the simulations. As shown in Fig. 6(a), the system flow rate for each urban-scale SALSCS with a

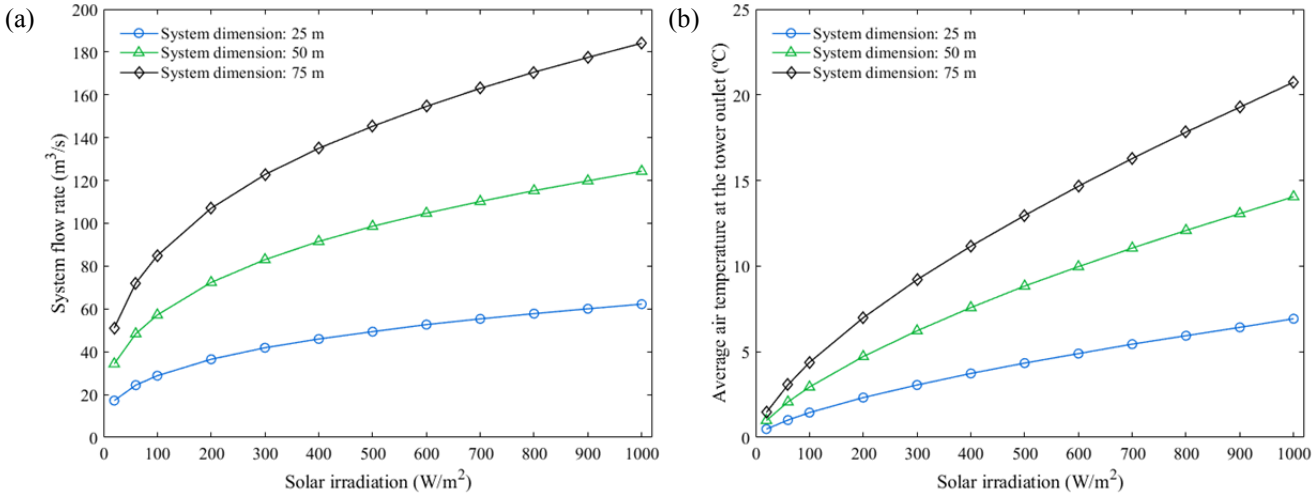

Fig. 3. Effects of solar irradiation on (a) SALSCS volumetric flow rate and (b) airflow temperature at the tower outlet, for three different system dimensions with fixed ambient and 2-m deep ground temperatures of 0°C and 4°C, respectively.

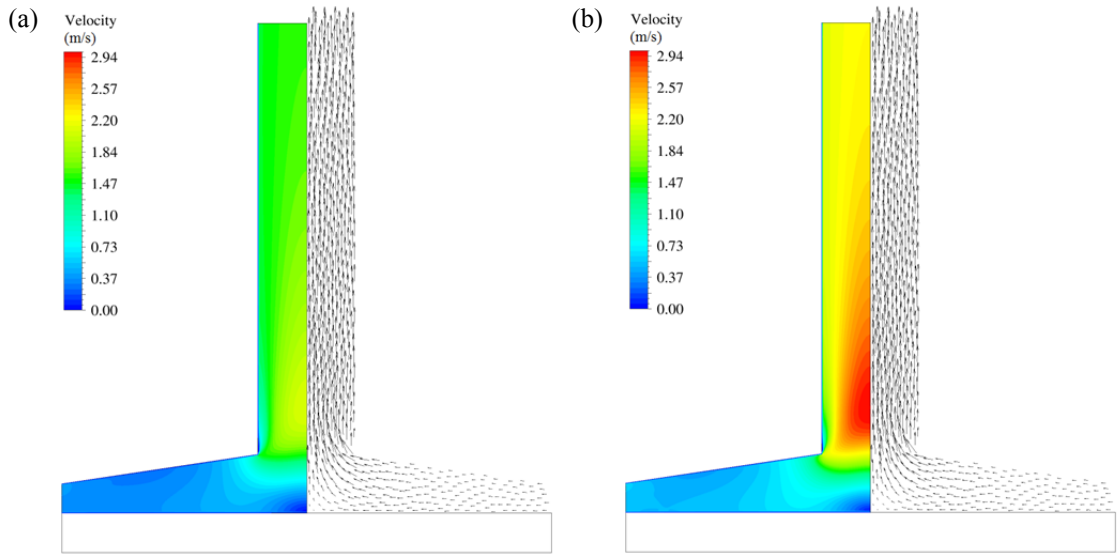

Fig. 4. Contour and vector plots for the velocity fields of an urban-scale SALSCS with same tower height and solar collector width of 25 m under two different ambient solar irradiations of (a) 200 W m^{-2} and (b) 600 W m^{-2}.

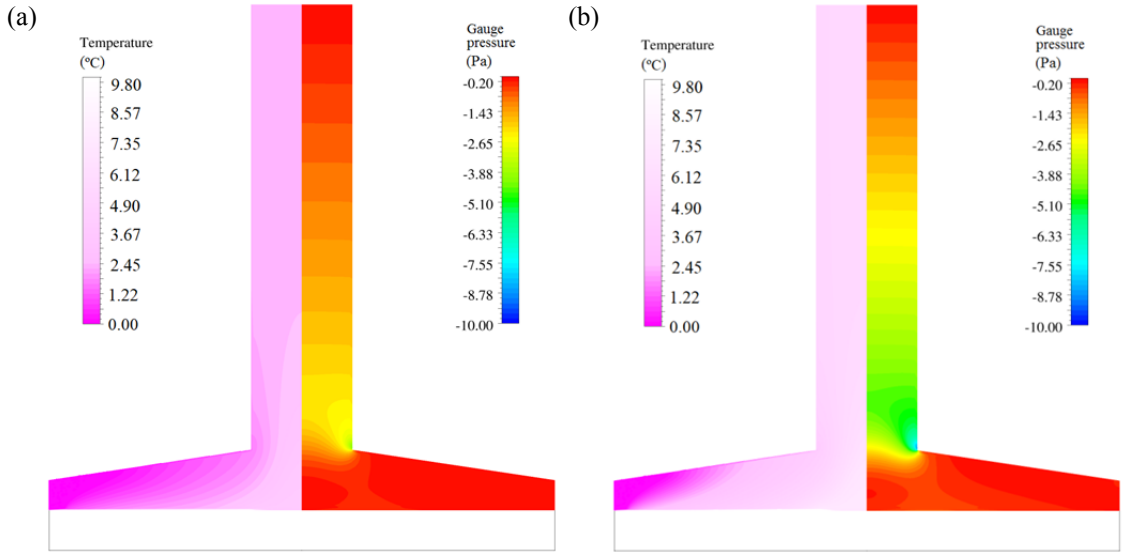

Fig. 5. Contour plots for the temperature and gauge static pressure fields of an urban-scale SALSCS with same tower height and solar collector width of 25 m at two different ambient solar irradiations of (a) 200 W m^{-2} and (b) 600 W m^{-2}.

specific system dimension barely changes with the ambient temperature. As the airflow field of SALSCS was assumed to be incompressible in the numerical model, according to the Boussinesq approximation (Spiegel and Veronis, 1960; Gray and Giorgini, 1976), the system flow field is driven by the temperature difference between the inside airflow and outside ambient environment and system air density has been assumed to be a constant equal to the air density of the nearby atmosphere. Therefore, by applying a fixed solar heat flux, the buoyance force, which drives the airflow field, would not be significantly varied at different ambient temperatures. In reality, under a higher ambient temperature, the airflow inside the system has a lower overall density and mass. Thus, with fixed solar irradiation applied, the system flow rate should be slightly higher with a higher ambient temperature. Further research should be conducted to analyze this effect in the future. In general, as indicated by our numerical results obtained from the incompressible model, the ambient temperature is not a factor with dominant influence on the SALSCS flow rate. It may be noticed that the Xi'an demonstration unit of SALSCS generates more airflow in the summer season than the winter season, which should mainly result from the higher solar irradiation intensity received by the solar collector instead of the increase in ambient temperature during summer time.

Although ambient temperature does not affect the system flow rate significantly, it has important influence on the airflow temperature inside the system. As presented by Fig. 6(b), there is a linear relationship between the

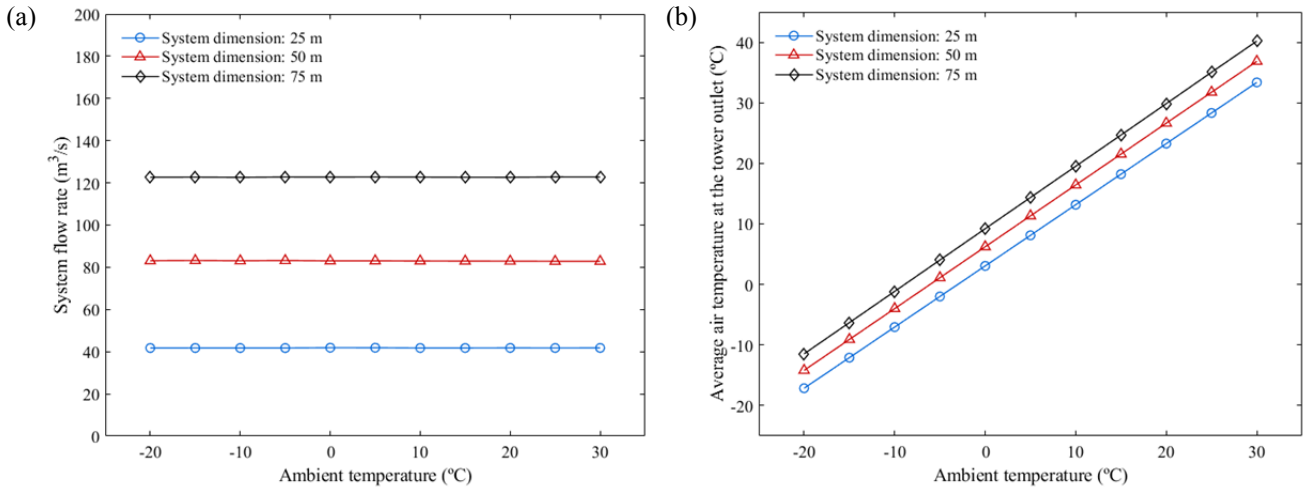

Fig. 6. Effects of ambient temperature on (a) volumetric system flow rate and (b) airflow temperature at the tower outlet, for three different system dimensions at a fixed ambient solar irradiation of 300 W m^{-2}, and 2-m deep ground temperature of 4°C.

airflow temperature at the tower outlet and the ambient temperature according to the numerical results. The reason is simply because the air flowing into the solar collector inlet has the same temperature as the ambient environment, and by raising the temperature at the system inlet, the overall system temperature should be increased accordingly. Fig. 6(b) also implies that a system with a larger solar collector area has higher airflow temperature due to the larger amount of solar energy received by the solar collector, whose effects on SALSCS performance will be discussed later in this paper.

2-m Deep Ground Temperature

Ground temperature fluctuates daily and annually affected mainly by variations in ambient air temperature and solar irradiation. According to Florides and Kalogirou (2005), ground temperature beyond 1 m under the earth's surface is usually insensitive to the diurnal cycle of ambient temperature and solar irradiation, but the annual variation of ground temperature can extend to a depth of around 10 m. Therefore, in this study we assumed the 2-m deep ground temperature as a constant in the numerical model of urban-scale SALSC, and investigated how the system flow rate changes within the range of annual fluctuation of the ground temperature. Wu and Nofziger (1999) presented a mathematical model to describe annual variations of daily average ground temperature at different depths, and validated the model against field observations at an experiment station located in the Hebei Province of northern China. According to their study, the daily average difference between the ground temperature at 1.6-m depth and the ambient air temperature in the northern China region is from about –9°C to 13°C during an annual cycle, and during winter seasons, the ground temperature below the earth's surface is typically higher than the ambient temperature. Thus, it is reasonable to assume the 2-m deep ground temperature as 4°C higher than the ambient environment when modelling the Xi'an demonstration unit during the wintertime as introduced previously. In the current investigation, the ambient temperature and solar irradiation were fixed at 0°C and 200 W m^{-2}, respectively, and the 2-m deep ground temperature in the numerical model varied from –10°C to 14°C. Density, specific heat and thermal conductivity of the soil layer were set to be 2000 kg m^{-3}, 1010 J kg^{-1} K^{-1} and 1.16 W m^{-1} K^{-1}, respectively. The system flow rate profiles as a function of the 2-m deep ground temperature for the three system dimensions are displayed in Fig. 7. By changing the ground temperature from –10°C to 14°C, the flow rates are only increased slightly by 0.9 m^3 s^{-1}, 1.7 m^3 s^{-1} and 2.0 m^3 s^{-1} for the three urban-scale SALSCSs with the same tower height and solar collector widths of 25 m, 50 m and 75 m, respectively. Therefore, according to the numerical results, the 2-m deep ground temperature does not have a significant effect on the SALSCS volumetric flow rate. The reason is that comparing to the temperature variations at 2-m deep under the ground, the solar heat flux applied at the ground surface is the dominant source for heating the air under the solar collector roof and driving the updraft airflow inside urban-scale SALSCS.

Effects of System Geometric Dimensions

In the current study, we are considering urban-scale SALSCS with a square solar collector and a tower in a shape of rectangular prism, whose geometry can be perfectly defined by the five geometric variables, including collector inlet height, collector outlet height, collector width, tower width and tower height, with three of them related with the solar collector and two of them related with the system tower. Parametric studies on each of the geometric variable are presented in the following sections. For the numerical simulations carried out in this section, ambient air temperature and solar irradiation were set to be 0°C and 350 W m^{-2}, respectively, and meanwhile, the 2-m deep ground temperature was chosen as 4°C higher than the ambient temperature.

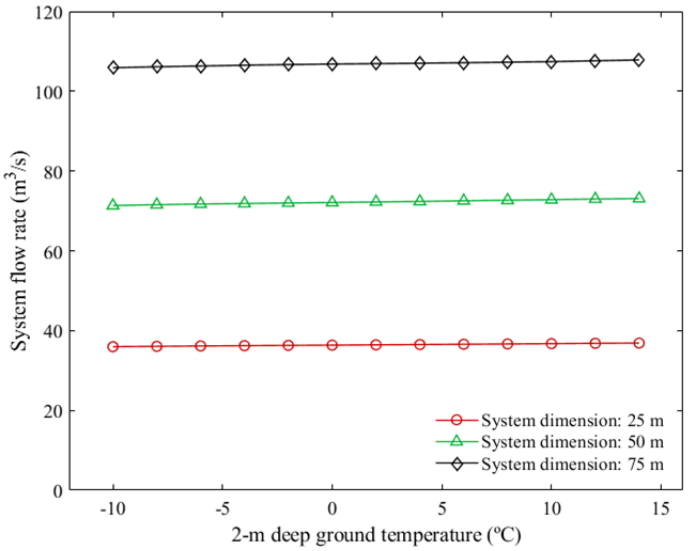

Fig. 7. Effect of 2-m deep ground temperature on SALSCS flow rate for three different system dimensions at fixed ambient temperature of 0°C, and ambient solar irradiation of 200 W m^{-2}.

Geometric Variables of Solar Collector

To study the influence of collector inlet and outlet heights on the system flow rate, we chose to perform numerical simulations on two urban-scale SALSCSs with the same tower height and solar collector width of 35 m and 70 m, respectively, while the tower width was fixed at 5 m for both the systems. To investigate the effect of the collector inlet height, for each urban-scale SALSCS, two height values of the solar collector outlet (or tower base height) were selected, which are 3 m and 5 m, respectively. The authors suggest that the collector inlet should always be lower than its outlet so that rain water on the solar collector can easily be drained down to the ground. Therefore, the collector inlet height was set to vary from 0.5 m to 2.5 m (or from 0.5 m to 4 m) for a fixed collector outlet height of 3 m (or 5 m). Fig. 8(a) indicates that the system flow rate slightly decreases with the inlet height of solar collector. For instance, by increasing the collector inlet height from 0.5 m to 4 m for a system with the same tower height and solar collector width of 70 m and a solar collector outlet height of 5 m, the flow rate is decreased by 7.9 m^3 s^{-1} (or 6%). Our conclusion based on the numerical simulations is consistent with the experimental findings by Ghalamchi *et al.* (2015), who reported that reducing the inlet size of a small SCPP has a positive effect on increasing the system power production. Fig. 8(a) also implies that the collector outlet height has a small but positive effect on the flow rate. To investigate the influence of the collector outlet height on the system performance, the inlet height was fixed at 1.5 m for both the two systems with dimensions of 35 m and 70 m. The dimensional range of 2–6 m for collector outlet height was tested, and the numerical results are presented in Fig. 8(b). By changing the collector outlet height from 2 m to 6 m, the system flow rate is increased by 2.1 m^3 s^{-1} (or 3.2%) for a system dimension of 35 m, and 4.3 m^3 s^{-1} (or 3.4%) for a system dimension of 70 m. The relationship between the system flow rate and the collector inlet and outlet heights can be attributed to the effect of the slope of the solar collector roof on the system airflow field. By lowering the collector inlet height or raising the collector outlet height, we are actually increasing this slope, which reduces the drag force from the collector roof exerting on the airflow field and slightly increases the system flow rate, since the warm air inside the solar collector always has a tendency of flowing upward. Our conclusion is that enhancing the inlet and outlet heights of the solar collector has negative and positive effects on the SALSCS volumetric flow rate, respectively. However, the overall effects of the two geometric variables on system performance are not significant.

The effects of solar collector width on SALSCS performance have also been considered by performing simulations on two urban-scale SALSCSs with different tower dimensions of 40 m in height with 5 m in width and 80 m in height with 10 m in width, respectively. The height of the solar collector was chosen to be increased from 2 m at the collector inlet to 5 m at the outlet. Fig. 9(a) presents the system flow rate profiles as a function of the width of the solar collector for the two systems, indicating that the solar collector width is an important factor affecting the flow rate and there is a roughly linear relationship between the two parameters. By increasing the width of the solar collector from 10 m to 120 m (or from 20 m to 120 m) for the tower of 40 m in height with 5 m in width (or 80 m in height with 10 m in width), the system flow rate is enhanced by 112.7 m^3 s^{-1} (or 327.4 m^3 s^{-1}). It is also implied by Fig. 9(a) that the system with an 80-m high and 10-m wide tower has a higher increasing gradient of system flow rate than the system with a 40-m high and 5-m wide tower, implying that a larger tower provides a higher potential for flow rate enhancement. In addition, the average airflow temperature at the system tower outlet increases significantly with the width of the solar collector, as presented by Fig. 9(b), resulting from the fact that a system

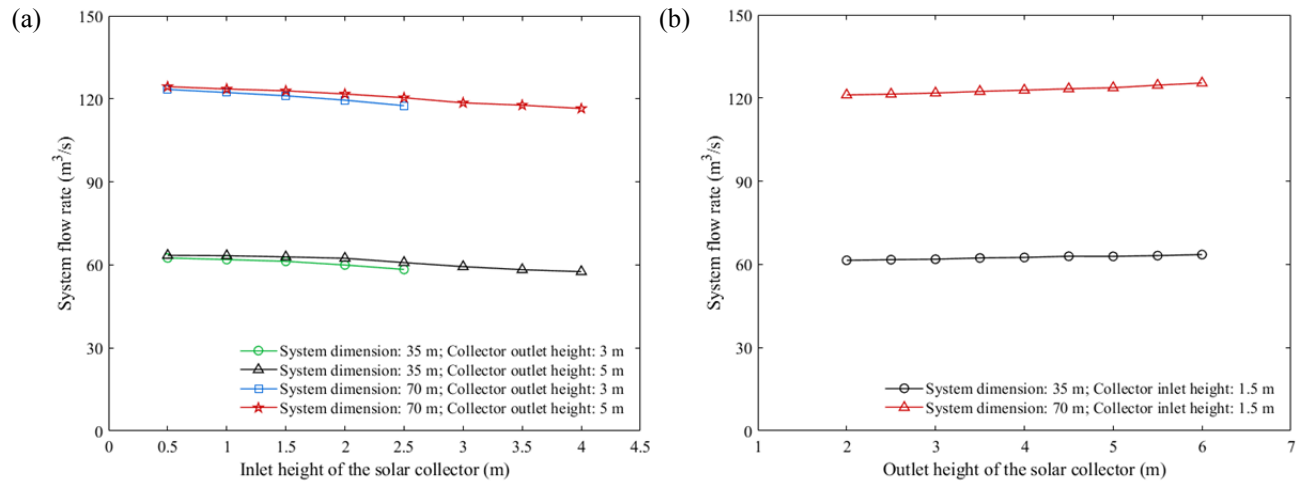

Fig. 8. Effects of solar collector (a) inlet height and (b) outlet height on the SALSCS flow rate for two different system dimensions at fixed ambient temperature of 0°C, ambient solar irradiation of 350 W m^{-2}, and 2-m deep ground temperature of 4°C.

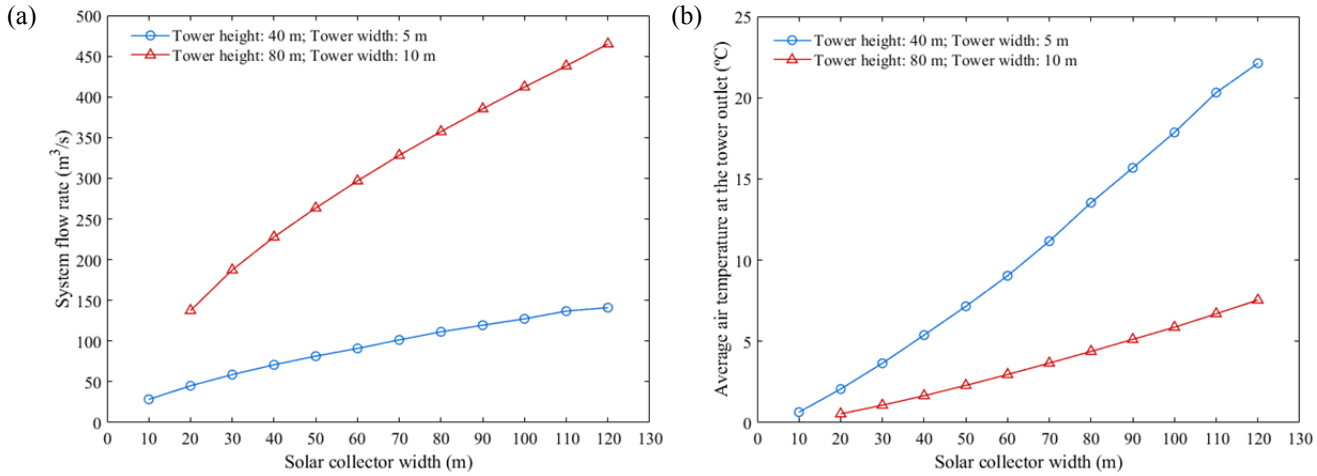

Fig. 9. Effects of solar collector width on (a) the system flow rate and (b) the airflow temperature at the tower outlet for two tower dimensions at fixed ambient temperature of 0°C, ambient solar irradiation of 350 W m^{-2}, and 2-m deep ground temperature of 4°C.

with a larger solar collector area receives more solar energy to raise up the airflow temperature. On the other hand, Fig. 9(b) shows that with the solar collector area staying as a constant, a system with a smaller tower dimension has an airflow field with higher overall temperature, since a smaller tower generates lower system flow rate which mitigates less heat away from the system during a certain time period.

Figs. 10(a) and 10(b) shows the velocity contours and vector plots for two urban-scale SALSCSs with a solar collector width of 40 m and 80 m, respectively, which have the same tower dimensions of 40 m in height and 5 m in width. The system with a larger solar collector area has a stronger velocity field, especially in the flow region inside the tower. The maximum local velocity equals to 3.8 m s^{-1} and 6.0 m s^{-1} for the SALSCSs with a collector width of 40 m and 80 m, respectively. Figs. 11(a) and 11(b) display the temperature and gauge static pressure contours for the two systems. The overall temperature field is higher for the system with a larger solar collector area. The lowest gauge static pressure appears at the connection region between the tower and solar collector, which equals to –17.2 Pa and –43.4 Pa for the systems with a solar collector width of 40 m and 80 m, respectively.

Although increasing the solar collector width can significantly improve the SALSCS volumetric flow rate as indicated by our study, considering the very limited construction space within an urban area, it is always easier to build an urban-scale SALSCS with a relatively small solar collector than a system with a large collector. Therefore, increasing solar collector width may not be a very economic approach to improve the system flow rate. Instead, we should put more effort into modifying the tower dimensions to realize a higher system flow rate for an urban-scale system. Thereby, influence of the parameters related with the system tower on SALSCS performance will be discussed in the following section.

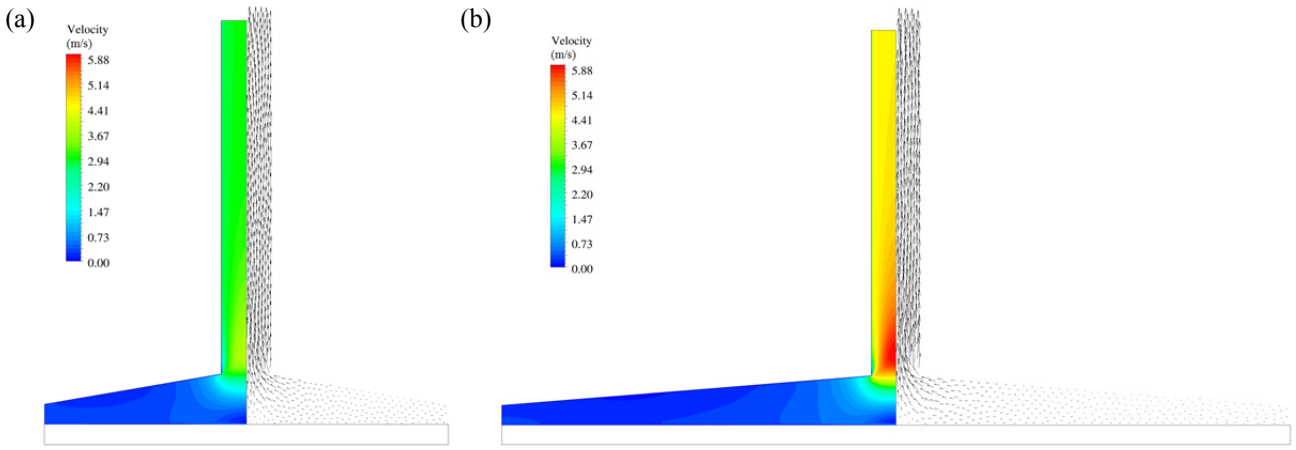

Fig. 10. Velocity contours and vector plots for two urban-scale SALSCSs with solar collector width of (a) 40 m and (b) 80 m, and same tower dimensions of 40 m in height and 5 m in width at ambient temperature of 0°C, ambient solar irradiation of 350 W m^{-2}, and 2-m deep ground temperature of 4°C.

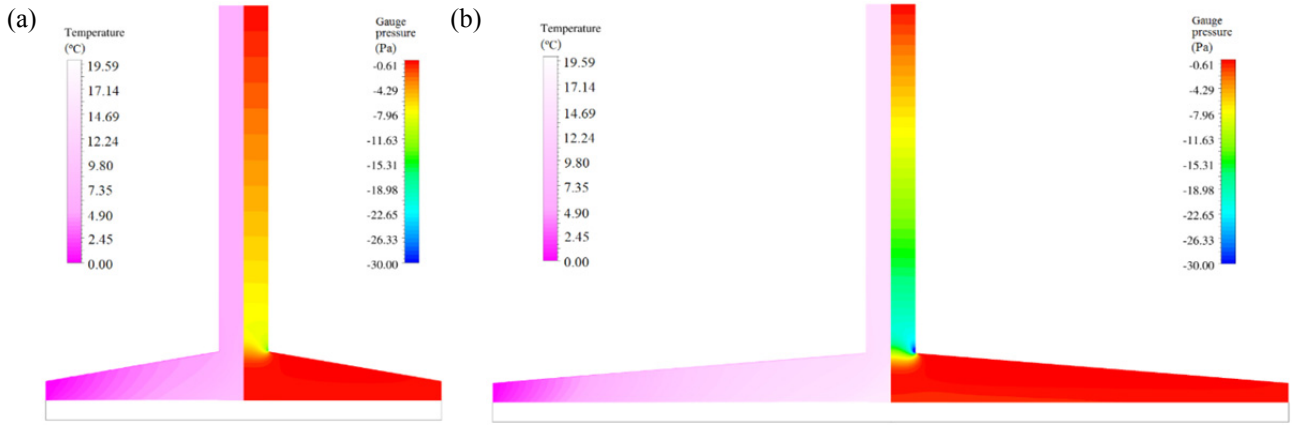

Fig. 11. Temperature and gauge static pressure contours for two urban-scale SALSCSs with solar collector width of (a) 40 m and (b) 80 m, and same tower dimensions of 40 m in height and 5 m in width at ambient temperature of 0°C, ambient solar irradiation of 350 W m^{-2}, and 2-m deep ground temperature of 4°C.

Geometric Variables of System Tower

There are two parametric variables related with the system tower, which are the tower width and height, respectively. Effects of the tower width on the system flow rate and average airflow temperature at the tower outlet are shown in Figs. 12(a) and 12(b), respectively. Two urban-scale SALSCSs with same solar collector width and tower height of 35 m and 70 m were utilized to study this effect. Both systems have the same solar collector heights of 2 m at the inlet and 5 m at the outlet. For each of the systems, we increased the tower width from 2 m to 12 m. As presented in Fig. 12(a), the system flow rate increases significantly with the tower width, showing that this parameter is essential to the performance of an urban-scale SALSCS. Within the test range of the tower width, the flow rate is enhanced by 176.0 m^3 s^{-1} and 366.8 m^3 s^{-1} for the two system dimensions of 35 m and 70 m, respectively. By comparing the two curves in Fig. 12(a), we also found a system with a larger solar collector and higher tower has a faster flow-rate increasing rate with the tower width. The effect of SALSCS tower width on the air temperature at the tower outlet is presented by Fig. 12(b). By increasing the tower width from 2 m to 12 m, the system with the same tower height and solar collector width of 35 m (or 70 m) has an outlet air temperature decreasing from 13.8°C to 1.4°C (or from 27.1°C to 3.0°C), which is due to that a larger system flow rate with a wider tower carries more heat away from the system flow field during a certain time period. Especially with a smaller tower width, the urban-scale SALSCS can have an airflow temperature much higher than the ambient environment.

The contour and vector plots for the system velocity fields of two urban-scale SALSCSs with a tower width of 4 m and 8 m are shown in Figs. 13(a) and 13(b), respectively, which have the same tower height and a solar collector width of 35 m. By increasing the tower width, the velocity field becomes weaker in the tower region but stronger in the collector region, which is due to the combined effect of increase in both the tower cross-section area and system flow rate. The maximum airflow velocity reaches to 3.7 m s^{-1} and 2.6 m s^{-1} for the two systems, respectively. The temperature and gauge static pressure contours for the two

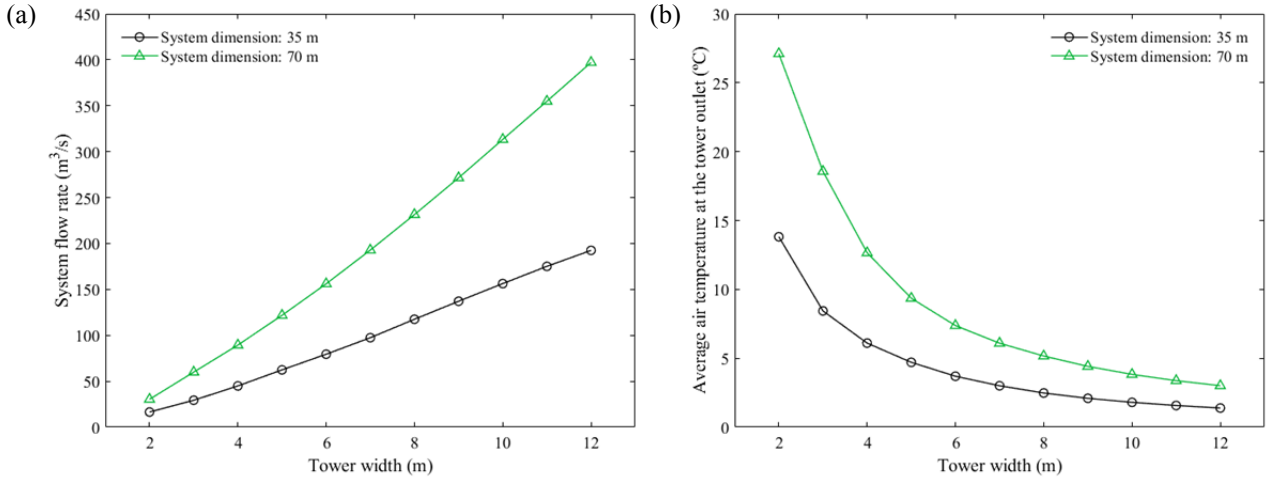

Fig. 12. Effects of tower width on (a) the SALSCS flow rate and (b) the airflow temperature at the tower outlet for two urban-scale SALSCSs with same tower height and collector width of 35 m and 70 m, respectively, at fixed ambient temperature of 0°C, solar irradiation of 350 W m^{-2}, and 2-m deep ground temperature of 4°C.

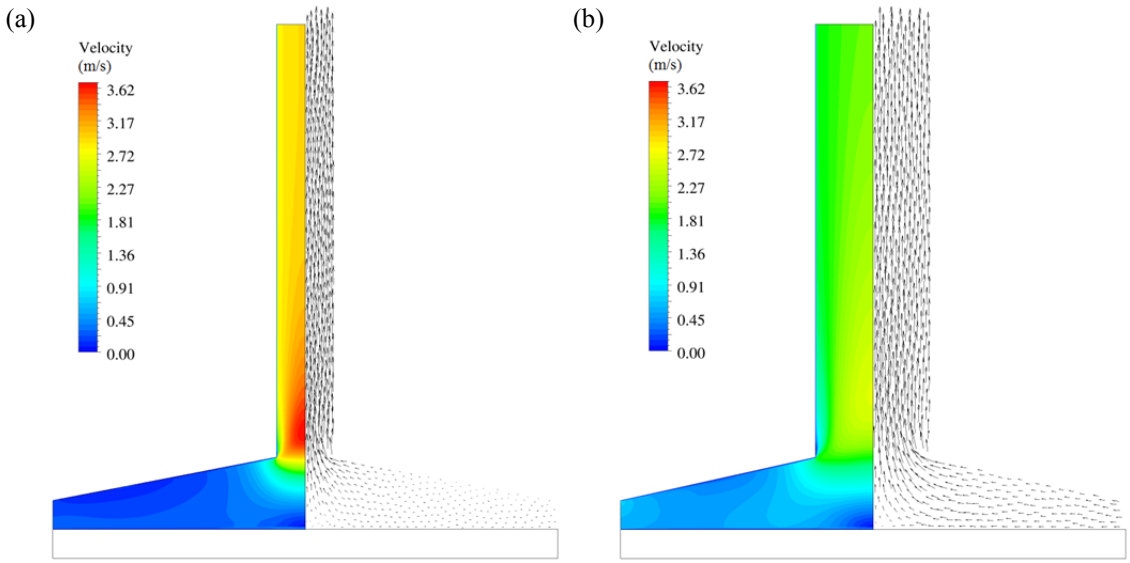

Fig. 13. Velocity contours and vector plots for two urban-scale SALSCSs with tower width of (a) 4 m and (b) 8 m, and same tower height and solar collector width of 35 m at ambient temperature of 0°C, ambient solar irradiation of 350 W m^{-2}, and 2-m deep ground temperature of 4°C.

systems are presented in Figs. 14(a) and 14(b), indicating that the system with a wider tower has a lower temperature field and a higher static pressure field. The minimum gauge static pressure magnitudes are –16.1 Pa and –8.0 Pa for the two urban-scale SALSCSs with a tower width of 4 m and 8 m, respectively.

The numerically-obtained system flow rate profiles as a function of the SALSCS tower height are displayed by the two curves with open markers in Fig. 15(a), where two systems with constant solar collector widths of 35 m and 70 m were simulated for the investigation. For both the systems, the tower width was fixed at 10 m, and the solar collector inlet and outlet heights were chosen to be 2 m and 5 m, respectively. Same with the tower width, the geometric variable of tower height also affects the system flow rate significantly. By increasing its value from 10 m to 120 m, the flow rate is increased by 147.0 m^3 s^{-1} (or 230.1 m^3 s^{-1}) for the system with a solar collector width of 35 m (or 70 m). Fig. 15(a) also indicates that with a larger system solar collector, the flow rate has a higher increasing rate with the tower height, which is consistent with the numerical results presented in Fig. 9(a).

The physics behind the relationship between system flow rate and tower height can be explained by the theoretical analysis as follows. SALSCS utilizes the buoyancy principle to generate updraft airflow inside the tower. Here we assume that the system geometry is only composed of a rectangular or cylindrical tower in the atmosphere with a cross-section area of A_c and height of H, and ignore the geometrical part of the solar collector. The buoyancy force,

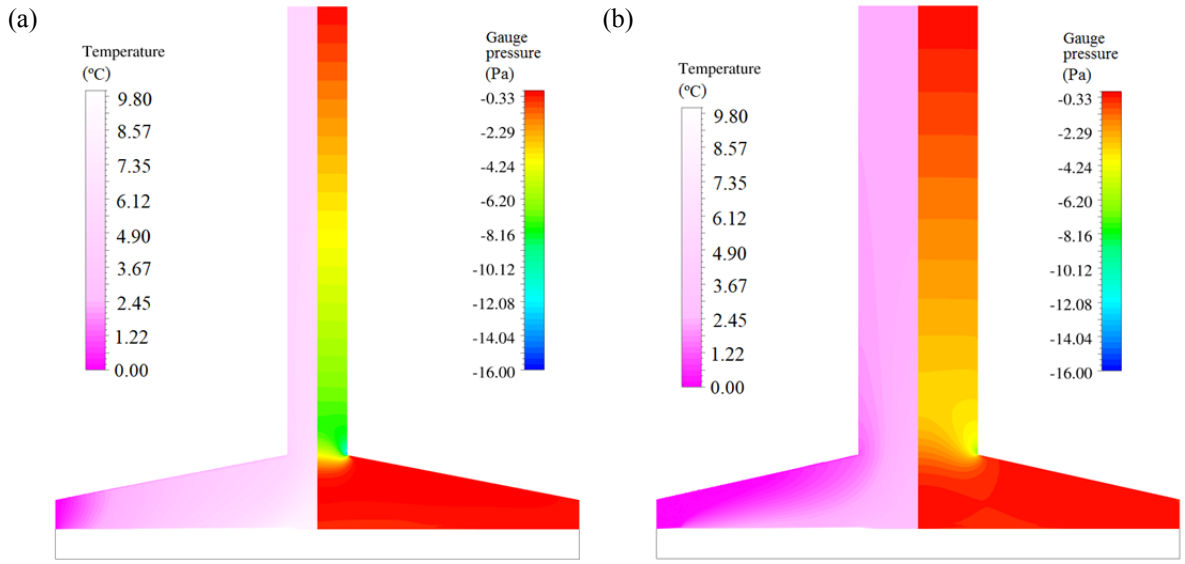

Fig. 14. Temperature and gauge static pressure contours for two urban-scale SALSCSs with tower width of (a) 4 m and (b) 8 m, and same tower height and solar collector width of 35 m at ambient temperature of 0°C, ambient solar irradiation of 350 W m^{-2}, and 2-m deep ground temperature of 4°C.

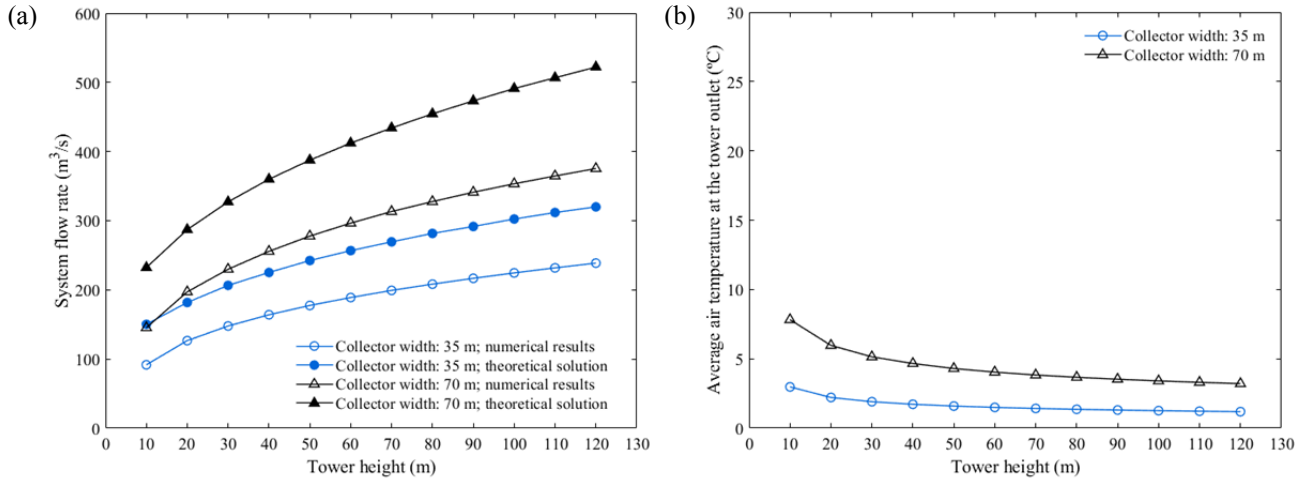

Fig. 15. Effects of tower height on (a) the system flow rate and (b) the airflow temperature at the tower outlet for two urban-scale SALSCSs with collector width of 35 m and 70 m, respectively, at fixed ambient temperature of 0°C, solar irradiation of 350 W m^{-2}, and 2-m deep ground temperature of 4°C.

B, and gravitational force, G, exerted on the air inside the tower are then given by the following two equations:

$$B = \rho_{\infty} g(A_c \cdot H) \tag{1}$$

$$G = \rho_a g(A_c \cdot H) \tag{2}$$

where g is the gravitational acceleration, ρ_{∞} the air density of the atmosphere, and ρ_a the density of the airflow inside the system tower. Because of solar heating, ρ_a is less than ρ_{∞}. Thus, the driving force for the updraft airflow, D, is written as:

$$D = B - G = (\rho_{\infty} - \rho_a) g(A_c \cdot H). \tag{3}$$

The corresponding pressure difference driving the airflow is then given by:

$$\Delta p = \frac{D}{A_c} = (\rho_{\infty} - \rho_a) gH \,, \tag{4}$$

which indicates that Δp is proportional to the tower height, H. According to Bernoulli's principle, this pressure drop is expressed as:

$$\Delta p = \frac{1}{2} \rho_a v_a^{\,2} \,, \tag{5}$$

where v_a is the airflow velocity inside the tower and is

written as:

$$v_a = \sqrt{\frac{2\Delta p}{\rho_a}}. \quad (6)$$

Therefore, the system volumetric flow rate, $\dot{V}$, is derived as:

$$\dot{V} = A_c \cdot v_a = A_c \sqrt{\frac{2\Delta p}{\rho_a}} = A_c \sqrt{2gH\frac{(\rho_\infty - \rho_a)}{\rho_a}} \quad (7)$$

According to Eq. (7), the system flow rate is linearly proportional to the square root of the tower height. In Fig. 15(a), the two curves with filled markers are system flow rates at different tower heights calculated theoretically by Eq. (7). Comparison between the curves with open and filled markers indicates that the numerical results follow the trend of the theoretical predictions. And difference between the two is mainly due to that the theoretical analysis ignores the drag force exerted on the SALSCS airflow field by the solar collector and tower walls.

Temperature effect of the tower height is shown in Fig. 15(b). At a tower width of 10 m, the airflow temperature at the tower outlet is only reduced by 1.8°C (or 4.6°C) for a system with a solar collector width of 35 m (or 70 m) after the tower height is increased from 10 m to 120 m. Comparing with tower width, the geometric variable of tower height does not have a dominant effect on reducing the system air temperature at a tower width of 10 m.

Figs. 16(a) and 16(b) present the velocity contours and vector plots for two systems with tower heights of 40 m and 80 m, respectively. Widths of the tower and solar collector are fixed at 10 m and 70 m, respectively. With a higher system tower, the velocity field is stronger in both solar collector and tower regions, due to a higher system flow rate. The flow field has a maximum local velocity in the tower region equal to 3.8 m s^{-1} and 4.8 m s^{-1} for the two systems, respectively. Figs. 17(a) and 17(b) show the temperature and gauge static pressure contours. The system with an 80-m tower has a slightly lower temperature field than the system with a 40-m tower. The gauge static pressure reaches the minimum value of –17.2 Pa and –43.4 Pa for the systems with a tower height of 40 m and 80 m, respectively.

As a conclusion, the study shows both the two geometric variables related with tower dimensions have significant influence on the performance of urban-scale SALSCS. As mentioned previously, it is a much more economic approach to increase the tower dimensions than the solar collector width for system flow rate improvement. One thing to be noted is that, if the tower is built with non-transparent material, such as concrete, a tower with large width or height may block away a large portion of solar irradiation from the solar collector during the day time, which may have a detrimental effect on the system flow-rate generation. However, if the tower is constructed with transparent material, such as glass, allowing the sunlight to pass through the tower walls and thereby heat the ground under the solar collector, then increasing the tower dimensions is a very effective method to increase the system flow rate.

Effects of Pressure Drop across Filters

To investigate the influence of pressure drop of installed filters on system performance, numerical simulations were carried out with filters modeled as an interface with constant pressure drop located at the mid-way between the solar collector inlet and centerline of the system tower, as mentioned in Section 5. Two different urban-scale SALSCSs were simulated with the same tower height and solar collector width of 35 m and 70 m, respectively. Other geometric dimensions were same for the two systems. The solar

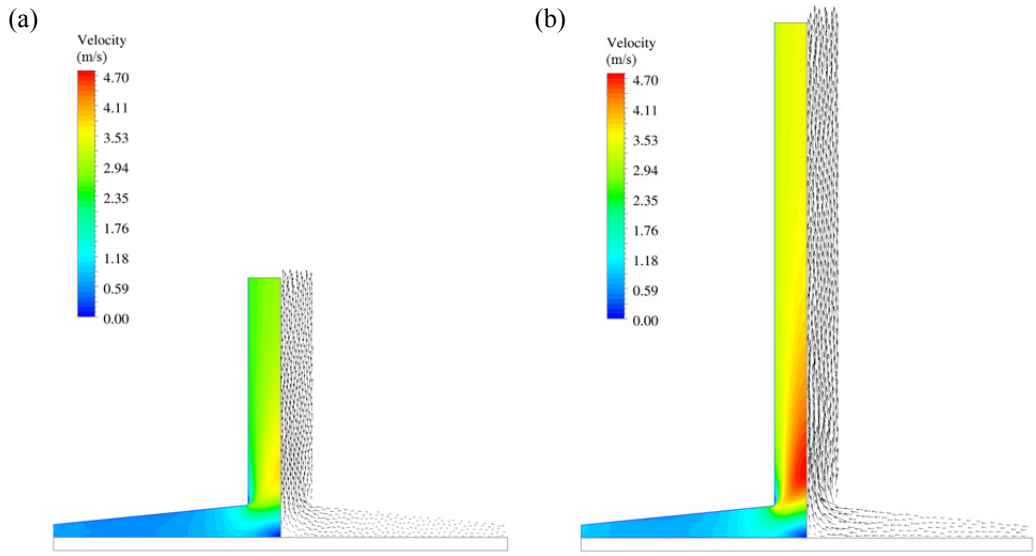

Fig. 16. Velocity contours and vector plots for two urban-scale SALSCSs with tower height of (a) 40 m and (b) 80 m, and same tower and solar collector widths of 10 m and 70 m, respectively, at ambient temperature of 0°C, ambient solar irradiation of 350 W m^{-2}, and 2-m deep ground temperature of 4°C.

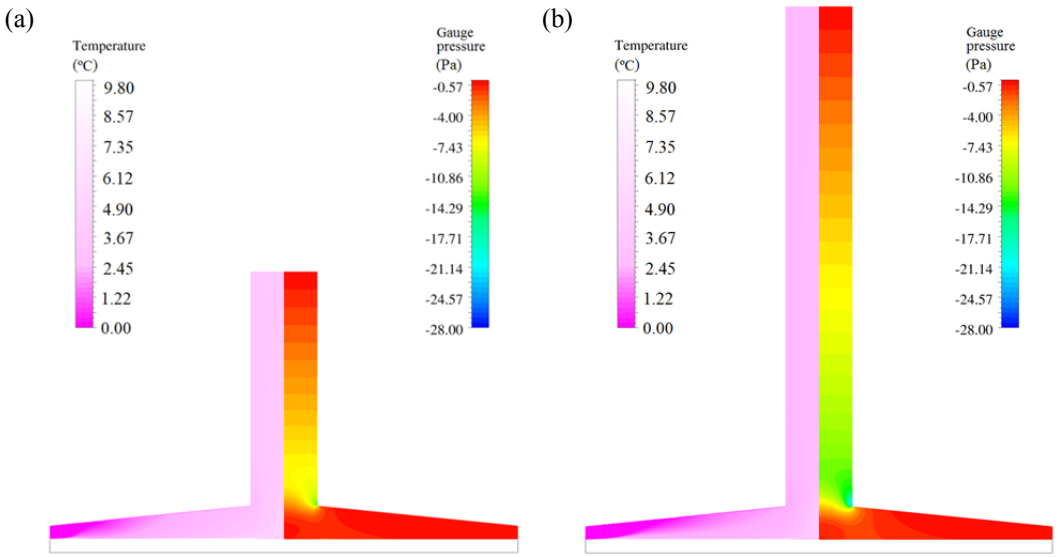

Fig. 17. Temperature and gauge static pressure contours for two urban-scale SALSCSs with tower height of (a) 40 m and (b) 80 m, and same tower and solar collector widths of 10 m and 70 m, respectively, at ambient temperature of 0°C, ambient solar irradiation of 350 W m^{-2}, and 2-m deep ground temperature of 4°C.

collector has an inlet height of 2 m and outlet height of 5 m, respectively, while the tower width was set to be 10 m. The ambient and 2-m deep ground temperatures were set to be 0°C and 4°C, respectively, for all simulations. Three ambient solar irradiation values of 350 W m^{-2}, 700 W m^{-2} and 1050 W m^{-2} were tested in this study. As shown in Fig. 18, the system flow rate at each solar irradiation value decreases almost linearly with the pressure drop across the filters until a critical pressure drop is reached, at which the airflow field of the system cannot overcome the filters anymore, resulting in zero flow rate in the system. According to the numerical results, for a system with the same tower height and solar collector width of 35 m (or 70 m), the critical pressure drop is equal to 5 Pa (or 11 Pa), 7 Pa (or 19 Pa) and 8 Pa (or 29 Pa) at a solar irradiation of 350 W m^{-2}, 700 W m^{-2} and 1050 W m^{-2}, respectively. By increasing the system dimensional scale or solar irradiation intensity, the airflow field within an urban-scale system is able to overcome filters with higher pressure drop. During the design process of filters for an urban-scale SALSCS, this issue has to be considered in order to make sure that under certain ambient conditions, filter pressure drop should always be lower than the corresponding critical value so that airflow generated by SALSCS can be maintained by solar heating. Otherwise, fans should be installed in the system to keep the system under operation consistently.

SUMMARY AND FUTURE WORK

In this paper, we present a parametric study on the urban-scale SALSCS—defined as having a dimensional range between 10 m and 120 m both horizontally and vertically—which can be deployed in large numbers on city blocks. The effects of different ambient and geometric variables on system performance were studied using the numerical model, which was validated against the experimental measurements introduced in Part I. The most influential parameters were identified as the ambient solar irradiation, solar collector width, tower width and tower height. The effects of the filters proposed for installation in the system were also evaluated by simulating the filters as an interface with a constant pressure drop located mid-way between the solar collector inlet and the tower centerline. The numerical results indicate that by varying solar irradiation from 20 W m^{-2} to 1000 W m^{-2}, the system flow rate is increased by 45.0 m^3 s^{-1}, 90.0 m^3 s^{-1} and 133.0 m^3 s^{-1} for three simulated systems when the tower height is identical and the solar collector widths are 25 m, 50 m and 75 m, respectively. Additionally, the airflow temperature significantly increases with the solar irradiation. The study also found that the influence of the ambient and the 2-m deep ground temperature on the system flow rate is not comparable to that of solar irradiation. Of the geometric parameters, the solar collector width, tower width and tower height all have significant and positive effects on the system's ability to generate updrafts. For instance, if the tower width is increased from 2 m to 12 m, the volumetric flow rate is enhanced by 366.8 m^3 s^{-1} for a system with an unchanged tower height and a collector width of 70 m. An urban-scale SALSCS with larger dimensions for these three geometric variables has a higher potential for flow rate enhancement, which also significantly impacts the temperature field of the system. The study also identified that a critical pressure drop for filters exists for a specific system dimension and ambient condition. If the filter pressure drop is higher than the critical value, the airflow field generated by solar energy cannot be maintained unless fans are installed to further strengthen the flow field.

Other parameters exist that have a considerable influence on the performance of an urban-scale SALSCS, such as the ground materials under the solar collector, the optical properties of the collector's transparent roof and the ambient

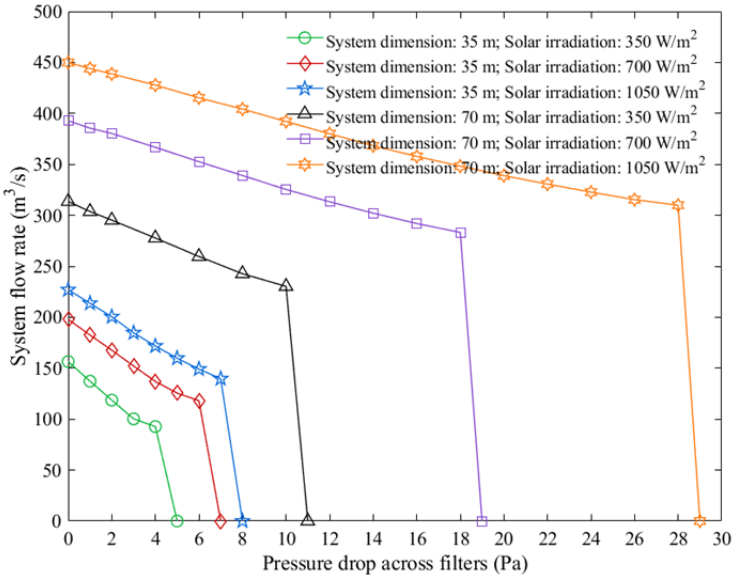

Fig. 18. Effect of pressure drop across filters on the system performance in generating airflow for two urban-scale SALSCSs under three ambient solar irradiation values of 350 W m^{-2}, 700 W m^{-2} and 1050 W m^{-2}.

wind. Investigations of these parameters involve different numerical models and experimental techniques, which are not covered in this paper but may be presented in future publications.

ACKNOWLEDGEMENTS

The authors would like to thank Professor Wojciech Lipiński from the Australian National University and Mr. Charles Lo from the University of Minnesota, respectively, for their suggestions on this work. Our numerical simulations were performed on the High-Performance Computing (HPC) platforms of the Minnesota Supercomputing Institute (MSI), which is also gratefully acknowledged.

NOMENCLATURE

A_c cross-section area, m^2.
B buoyancy force, kg m^{-1} s^{-2}.
D driving force for SALSCS updraft airflow, kg m^{-1} s^{-2}.
G gravitational force, kg m^{-1} s^{-2}.
g gravitational acceleration, m s^{-2}.
H tower height, m.
h convective heat transfer coefficient, W m^{-2} K^{-1}.
$\dot{V}$ volumetric system flow rate, m^3 s^{-1}.
q heat flux, W m^{-2}.
v_a airflow velocity in SALSCS tower, m s^{-1}.

Greek

Δp pressure drop, Pa.
ρ_∞ air density of the atmosphere, kg m^{-3}.
ρ_a air density in the system tower, kg m^{-3}.

REFERENCES

Ayadi, A., Bouabidi, A., Driss, Z. and Abid, M.S. (2018). Experimental and numerical analysis of the collector roof height effect on the solar chimney performance. *Renew. Energy* 115: 649–662.

Becerra, T.A., Wilhelm, M., Olsen, J., Cockburn, M. and Ritz, B. (2013). Ambient air pollution and autism in Los Angeles County, California. *Environ. Health Perspect.* 121: 380–386.

Brook, R.D., Rajagopalan, S., Pope, C.A., Brook, J.R., Bhatnagar, A., Diez-Roux, A.V., Holguin, F., Hong, Y., Luepker, R.V., Mittleman, M.A., Peters, A., Siscovick, D., Smith, S.C., Whitsel, L. and Kaufman, J.D. (2010). Particulate matter air pollution and cardiovascular disease: An update to the scientific statement from the American heart association. *Circulation* 121: 2331–2378.

Cao, Q., Pui, D.Y.H. and Lipiński, W. (2015). A concept of a novel solar-assisted large-scale cleaning system (SALSCS) for urban air remediation. *Aerosol Air Qual. Res.* 15: 1–10.

Cao, Q., Shen, L., Chen, S.C. and Pui, D.Y.H. (2018). WRF modeling of $PM_{2.5}$ remediation by SALSCS and its clean air flow over Beijing terrain. *Sci. Total Environ.* 626: 134–146.

Chan, C.K. and Yao, X. (2008). Air pollution in mega cities in China. *Atmos. Environ.* 42: 1–42.

de Richter, R.K., Ming, T.Z. and Caillol, S. (2013). Fighting global warming by photocatalytic reduction of CO_2 using giant photocatalytic reactors. *Renewable Sustainable Energy Rev.* 19: 82–106.

Federal Register (2006) Federal Register 61144. National ambient air quality standards for particulate matter. Federal Register October 17, 2006/Rules and Regulations; 71(200).

Feng, L. and Liao, W. (2016). Legislation, plans, and policies for prevention and control of air pollution in China: Achievements, challenges, and improvements. *J. Clean. Prod.* 112: 1549–1558.

Florides, G.A. and Kalogirou, S.A. (2005). Annual ground temperature measurements at various depths. Proceedings of CLIMA 2005, Lausanne, Switzerland.

Gao, J., Yuan, Z., Liu, X., Huang, X. and Dong, Z. (2016). Improving air pollution control policy in China - A perspective based on cost-benefit analysis. *Sci. Total Environ*. 543: 307–314.

Genc, S., Zadeoglulari, Z., Fuss, S.H. and Genc, K. (2012). The adverse effects of air pollution on the nervous system. *J. Toxicol*. 2012: 782462–782484.

Ghalamchi, M., Kasaeian, A. and Ghalamchi, M. (2015). Experimental study of geometrical and climate effects on the performance of a small solar chimney. *Renewable Sustainable Energy Rev*. 43: 425–431.

Ghalamchi, M., Kasaeian, A., Ghalamchi, M. and Mirzahosseini, A.H. (2016). An experimental study on the thermal performance of a solar chimney with different dimensional parameters. *Renewable Energy* 91: 477–483.

Gong, T., Ming, T., Huang, X., de Richter, R.K., Wu, Y. and Liu, W. (2017). Numerical analysis on a solar chimney with an inverted U-type cooling tower to mitigate urban air pollution. *Sol. Energy* 147: 68–82.

Gray, D.D. and Giorgini, A. (1976). The validity of the Boussinesq approximation for liquids and gases. *Int. J. Heat Mass Transfer* 19: 545–551.

Guan, W.J., Zheng, X.Y., Chung, K.F. and Zhong, N.S. (2016). Impact of air pollution on the burden of chronic respiratory diseases in China: time for urgent action. *Lancet* 388: 1939–1951.

Hassan, A., Ali, M. and Waqas, A. (2018). Numerical investigation on performance of solar chimney power plant by varying collector slope and chimney diverging angle. *Energy* 142: 411–425.

He, K., Huo, H. and Zhang, Q. (2003). Urban air pollution in China: Current status, characteristics, and progress. *Annu. Rev. Energy Environ*. 27: 397–431.

Hoek, G., Krishnan, R.M., Beelen, R., Peters, A., Ostro, B., Brunekreef, B. and Kaufman, J.D. (2013). Long-term air pollution exposure and cardio-respiratory mortality: A review. *Environ. Health* 12: 43.

Huang, R.J., Zhang, Y., Bozzetti, C., Ho, K.F., Cao, J.J., Han, Y., Daellenbach, R.K., Slowik, J.G., Platt, S.M., Canonaco, F., Zotter, P., Wolf, R., Pieber, S.M., Bruns, E.A., Crippa, M., Ciarelli, G., Piazzalunga, A., Schwikowski, M., Abbaszade, G., Schnelle-Kreis, J., Zimmermann, R., An, Z., Szidat, S., Baltensperger, U., Haddad, I.E. and Prévôt, A.S.H. (2014). High secondary aerosol contribution to particulate pollution during haze events in China. *Nature* 514: 218–222.

Kan, H., Chen, R. and Tong, S. (2012). Ambient air pollution, climate change, and population health in China. *Environ. Int*. 42: 10–19.

Kasaeian, A., Mahmoudi, A.R., Astaraei, F.R. and Hejab, A. (2017). 3D simulation of solar chimney power plant considering turbine blades. *Energy Convers. Manage.* 147: 55–65.

Kasaeian, A.B., Heidari, E. and Nasiri Vatan, Sh. (2011). Experimental investigation of climatic effects on the efficiency of a solar chimney pilot power plant. *Renewable Sustainable Energy Rev*. 15: 5202–5206.

Li, J.Y., Guo, P.H. and Wang, Y. (2012). Effects of collector radius and chimney height on power output of a solar chimney power plant with turbines. *Renewable Energy* 47: 21–28.

Maia, C.B., Ferreira, A.G., Valle, R.M. and Cortez, M.F.B. (2009). Theoretical evaluation of the influence of geometric parameters and materials on the behavior of the air flow in a solar chimney. *Comput. Fluids* 38: 625–636.

Ming, T.Z., de Richter, R.K., Meng, F.L., Pan, Y. and Liu, W. (2011). Chimney shape numerical study for solar chimney power generating systems. *Int. J. Energy Res*. 37: 310–322.

Ming, T.Z., Wang, X., de Richter, R.K., Liu, W., Wu, T. and Pan, Y. (2012). Numerical analysis on the influence of ambient crosswind on the performance of solar updraft power plant system. *Renewable Sustainable Energy Rev*. 16: 5567–5583.

Ming, T.Z., de Richter, R., Shen, S. and Caillol, S. (2016). Fighting global warming by greenhouse gas removal: destroying atmospheric nitrous oxide thanks to synergies between two breakthrough technologies. *Environ. Sci. Pollut. Res*. 23: 6119–6138.

Patel, S.K., Prasad, D. and Ahmed, M.R. (2014). Computational studies on the effect of geometric parameters on the performance of a solar chimney power plant. *Energy Convers. Manage.* 77: 424–431.

Song, C., Wu, L., Xie, Y., He, J., Chen, X., Wang, T., Lin, Y., Jin, T., Wang, A., Liu, Y., Dai, Q., Liu, B., Wang, Y. and Mao, H. (2017). Air pollution in China: Status and spatiotemporal variations. *Environ. Pollut*. 227: 334–347.

Spiegel, E.A. and Veronis, G. (1960). On the Boussinesq Approximation for a Compressible Fluid. *Astrophys. J.* 131: 442–447.

Suades-González, E., Gascon, M., Guxens, M. and Sunyer, J. (2015). Air pollution and neuropsychological development: A review of the latest evidence. *Endocrinology* 156: 3473–3482.

Sun, C., Yuan, X. and Yao, X. (2016). Social acceptance towards the air pollution in China: Evidence from public's willingness to pay for smog mitigation. *Energy Policy* 92: 313–324.

Tan, D., Zhou, X., Xu, Y., Wu, C. and Li, Y. (2017). Environmental, health and economic benefits of using urban updraft tower to govern urban air pollution. *Renewable Sustainable Energy Rev.* 77: 1300–1308.

Watts, J. (2005). China: The air pollution capital of the world. *Lancet* 366: 1761–1762.

Wu, J. and Nofziger, D.L. (1999). Incorporating temperature effects on pesticide degradation into a management model. *J. Environ. Qual*. 28: 92–100.

Yu, S.C. (2014). Water spray geoengineering to clean air pollution for mitigating haze in China's cities. *Environ. Chem. Lett*. 12: 109–116.

Zhang, J., Reid, J.S., Alfaro-Contreras, R. and Xian, P. (2017). Has China been exporting less particulate air

pollution over the past decade? *Geophys. Res. Lett*. 44: 2941–248.

Zhao, S., Yu, Y., Yin, D., He, J., Liu, N., Qu, J. and Xiao, J. (2016). Annual and diurnal variations of gaseous and particulate pollutants in 31 provincial capital cities based on in situ air quality monitoring data from China national environmental monitoring center. *Environ. Int*. 86: 92–106.

Zhou, X.P., Yang, J.K., Xiao, B., Hou, G.X. and Xing, F. (2009). Analysis of chimney height for solar chimney power plant. *Appl. Therm. Eng*. 29: 178–185.

Zhou, X.P., Xu, Y.Y., Yuan, S., Wu, C. and Zhang, H. (2015). Performance and potential of solar updraft tower used as an effective measure to alleviate Chinese urban haze problem. *Renewable Sustainable Energy Rev*. 51: 1499–1508.

Received for review, June 28, 2018
Revised, August 31, 2018
Accepted, September 15, 2018